Nuclear Inst. and Methods in Physics Research, A 886 (2018) 30–35

Contents lists available at ScienceDirect

Nuclear Inst. and Methods in Physics Research, A

journal homepage: www.elsevier.com/locate/nima

Time-resolved gamma spectroscopy of single events

W. Wolszczak *, P. Dorenbos

Delft University of Technology, Faculty of Applied Sciences, Department of Radiation Science and Technology (FAME-LMR), Mekelweg 15, 2629 JB Delft, Netherlands

ARTICLE INFO

Keywords:
Time-resolved gamma spectroscopy
Pulse shape analysis
Data acquisition
Digital signal processing
Gamma spectroscopy
CsI(Tl)

ABSTRACT

In this article we present a method of characterizing scintillating materials by digitization of each individual scintillation pulse followed by digital signal processing. With this technique it is possible to measure the pulse shape and the energy of an absorbed gamma photon on an event-by-event basis. In contrast to time-correlated single photon counting technique, the digital approach provides a faster measurement, an active noise suppression, and enables characterization of scintillation pulses simultaneously in two domains: time and energy. We applied this method to study the pulse shape change of a CsI(Tl) scintillator with energy of gamma excitation. We confirmed previously published results and revealed new details of the phenomenon.

1. Introduction

Despite many years of studies on scintillating materials many questions are still open. While luminescence processes and high energy radiation interactions with matter are well understood, the fundamental processes of energy transport and high density quenching are still puzzling [1–6]. It is well known that a scintillation pulse shape changes with change of type of excitation (γ-rays, neutrons, α particles, high energy ions) [7–13]. This phenomenon is commonly used for particle discrimination in variety of applications [14–17]. However, the origin and the exact mechanism are still not known. In last years, a dependence of a scintillation pulse shape on γ photons energy was reported for various materials [18–21]. Recent theoretical developments [2,3,5,6] provided an explanation of these observations by modeling the charge separation inside the ionization track created during a gamma energy excitation.

Despite successful results of the theoretical modeling, many aspects still require an experimental study and verification. This raises a need for new data and a new experimental approach. The aim of this study is to provide a new method of characterizing scintillators in two domains simultaneously: in terms of the excitation energy, and time evolution of scintillation.

We will demonstrate that by digitization of individual scintillation pulses and digital signal processing it is possible to study the scintillation mechanism in terms of pulse shape and light yield at the same time. For each scintillation pulse it is possible to calculate the integral light output and corresponding deposited amount of energy. The acquired pulse height spectrum can be later subdivided into energy bins. An average scintillation pulse shape can be calculated for each energy bin by taking an average of all acquired events within that bin. However, to obtain undistorted pulse shapes additional signal processing and event selections are required before taking the average.

With this method we verified previous experimental results on CsI(Tl) pulse shape dependence on gamma energy, and we compared those results with theoretical models [6]. We have found that the pulse shape change predicted by the model is in good agreement with the measured data, however we observed some differences. The proposed method was used to characterize a scintillation decay time of CsI(Tl) excited with pulsed X-rays and gamma rays. It was found that X-ray pulses produce a significantly different pulse shape compared to single gamma events of an energy equal to the aggregate energy deposition of multiple lower-energy X-ray photons in the pulse. We will conclude that the proposed method provides a new way of characterization of scintillators.

2. Materials and methods

2.1. The setup

The measuring setup is shown diagrammatically in Fig. 1. Scintillation pulses from a one inch CsI(Tl) sample are converted to electrical pulses by a Hamamatsu H5510 Photomultiplier Tube (PMT). The scintillation crystal is optically coupled with silicon oil to the PMT's entrance window. The PMT's anode signal is connected directly to the 10-bit 4 Giga Samples Per Second (GSPS) DT5761 digitizer from CAEN.

* Corresponding author.
E-mail address: w.w.wolszczak@tudelft.nl (W. Wolszczak).

https://doi.org/10.1016/j.nima.2017.12.080
Received 15 December 2017; Received in revised form 28 December 2017; Accepted 30 December 2017
Available online 3 January 2018
0168-9002/

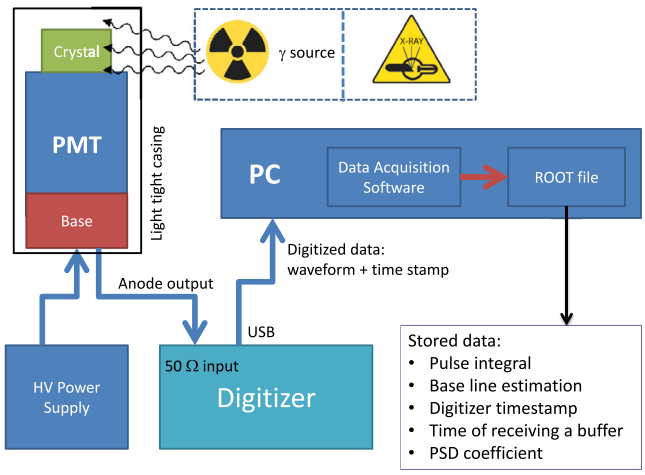

Fig. 1. Schematic of the time resolved Gamma spectroscopy setup. The gamma source or a pulsed X-ray tube excite the scintillation crystal. The resulting scintillation pulses are detected with a photomultiplier tube and digitized on event-by-event principle.

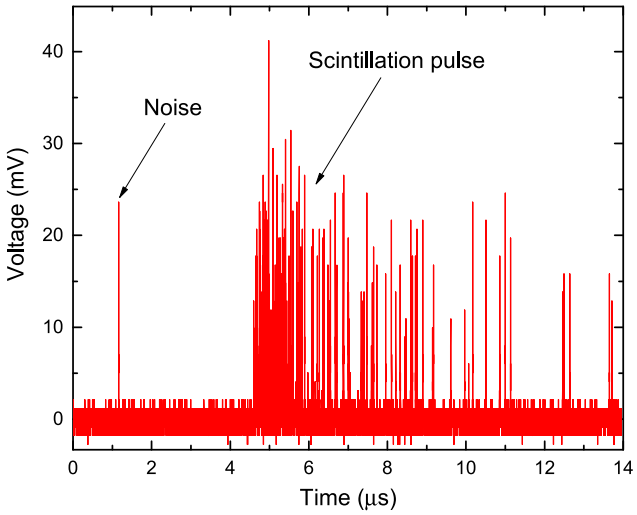

Fig. 2. Event triggered by a noise spike at around 1 μs with a coincident scintillation pulse starting at around 5 μs.

The digitizer has an input range of 1 Vpp, input impedance $Z_{in} = 50\Omega$, and a memory buffer depth of $7.2{\cdot}10^6$ samples. No preamplifier nor other ways of analog signal shaping have been used. All data acquisition and on-line processing is done with a personal computer and homemade software *veroDigitizer*.

A ^{137}Cs source has been used for excitation. The barium X-rays (32 keV) were absorbed by a lead absorber placed between the ^{137}Cs source and the detector. In this way we avoided photoelectric absorption of low energy X-rays, and only photoelectrons or Compton electrons from 662 keV gamma interaction were detected. As an alternative to γ rays, we used a light excited X-ray tube N5084 from Hamamatsu for generation of ultra short X-ray pulses (< 100 ps). The X-ray tube has a tungsten target and is powered with a 40 kV power supply. Each X-ray pulse contains multiple X-ray photons, which enables low energy excitation (~10 keV) but with a high light output.

2.2. Data acquisition

When the anode signal exceeds the digitizer's trigger voltage V_{tr} an event is triggered and stored in a local buffer. Each event contains a waveform consisting of 56 k voltage samples (14 μs time range). When the internal buffer is full, all digitized events are transferred to the PC for data processing. In order to record low energy events, the digitizer's trigger voltage V_{tr} was set as close as possible to the signal's base line. However, the low V_{tr} results in pick-up of noise spikes like in the exemplary pulse shown in Fig. 2. Fig. 3 shows the steps of the data processing which are required before the triggered events can be used for calculating average pulse shapes. Only events fulfilling multiple criteria are selected in order to remove unwanted noise events, suppress pile-up, and assure good quality of each triggered pulse. The following sections will discuss in detail each step of the data processing.

2.3. Filtering and decimation

The digitizer reduces a continuous-time signal from the PMT to a discrete-time digital signal (sampling). High sampling frequency of the used digitizer $f_s = 4$ GHz provides precise timing information, but in case of CsI(Tl) with slow decay time it results in high uncertainty of each value at a point in time of the measured signal (low signal to noise ratio). This can be seen in Fig. 2 and raw signal in Fig. 4. To increase the signal to noise ratio and decrease the uncertainty of a measured voltage each waveform was down-sampled (decimated) by first applying a low pass digital filter and then reducing the number of samples by a factor of $M = 256$.

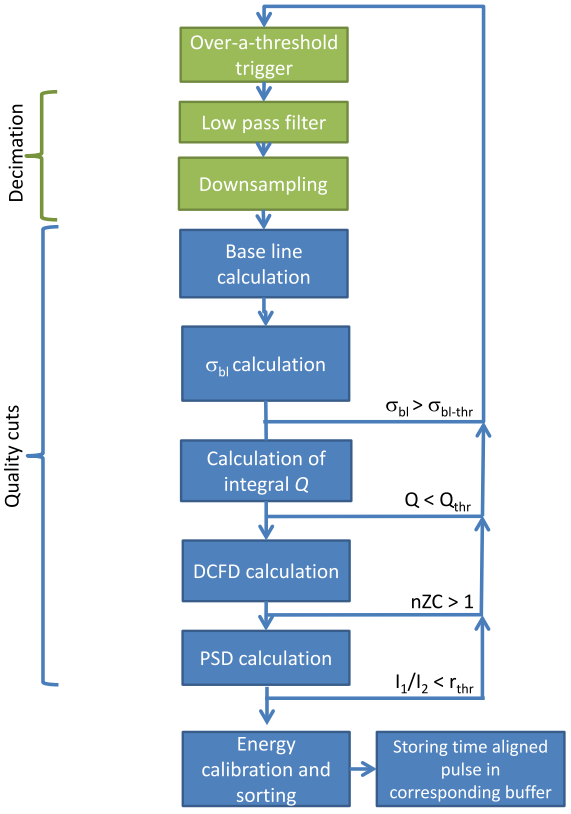

Fig. 3. Diagram of data processing workflow. σ_{bl} is the standard deviation of the base line; σ_{bl-thr} is a maximum threshold for standard deviation of the base line; Q is the pulse integral; Q_{thr} is a pulse integral minimum threshold; nZC is the number of zero crossings in the Digital Constant Fraction Discriminator (DCFD) signal; I_1/I_2 is the pulse shape factor defined as the ratio of the short and long integration gates.

To avoid aliasing it is needed to do a low pass filtering before downsampling [22]. The cutoff frequency of the filter has to be equal or lower than the Nyquist frequency of the down-sampled signal, which is $f_{co} = \frac{f_s/2}{M} = \frac{4000/2}{256} \approx 7.8$ MHz. Fig. 5 shows time and frequency domain responses of multiple standard digital filters designed for −3dB cutoff frequency at 7.8 MHz. Because in our measurements we want to preserve an undistorted time response of the signal, the filter choice

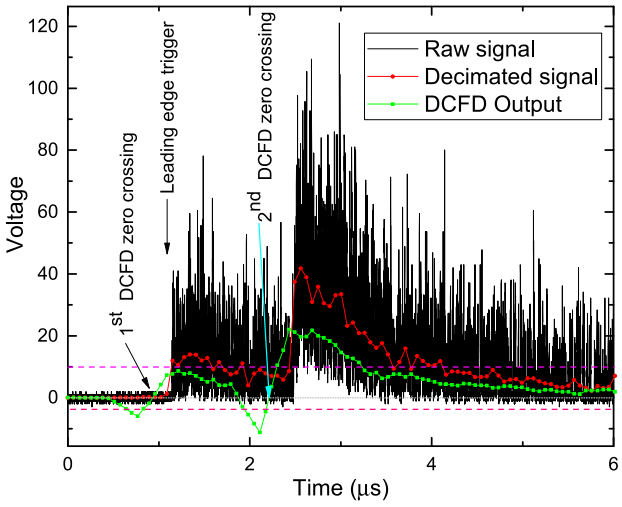

Fig. 4. Exemplary pile-up event. (For interpretation of the references to color in this figure legend, the reader is referred to the web version of this article.)

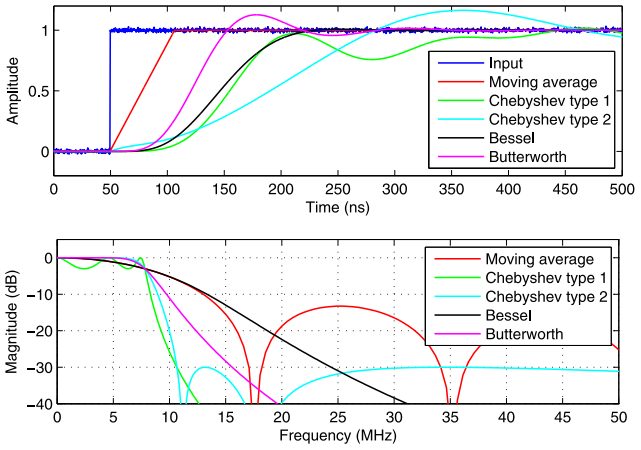

Fig. 5. Comparison of five digital low pass filters in time (upper panel) and frequency domains (lower panel). (Color online).

is limited just to two filters: a moving average filter (length N = 227) or a Bessel filter. The moving average filter has the worst frequency response among considered filters. It has side lobes in the stop band, but provides the fastest rise time in response to the step input, and it is free of overshoots in the time domain. In addition, a recursive implementation of the moving average filter provides the shortest computation time compared to that of the other filters [22]. The moving average filter was used for the results presented here.

Each sample of the downsampled waveform $d[i]$ is calculated by taking the average value of length $M = 256$ from the filtered waveform $f[i]$ according to the formula: $d[i] = \frac{1}{M}\sum_{k=M\cdot i}^{M\cdot(i+1)} f[i]$.

2.4. Quality cuts

Selections were applied to data to remove noise events, assure proper triggering time within each waveform, and to select non distorted single scintillation pulses. Fig. 3 shows the steps of the data processing. After an event decimation a baseline BL and its' standard deviation σ_{bl} are calculated. If σ_{bl} exceeds the base line standard deviation threshold σ_{bl-thr} the event is discarded and no longer processed. In this way we assure a good quality of the calculated base line. Usually σ_{bl-thr} is exceeded when random noise is present within the base line window or a scintillation pulse was triggered too late and the leading edge is before the expected triggering time.

In the next step the integral Q of a decimated pulse is calculated using the previously obtained base line: $Q = \sum_0^L (w[i] - BL)$. If the calculated Q is lower than the minimum integral threshold Q_{thr}, the event is discarded and no longer processed. This requirement suppresses all events which exceed the digitizer's trigger threshold, but consist mostly of noise spikes, single photoelectron events, afterglow pulses, or other non-scintillation pulses. This requirement is crucial especially for low energy deposition events when noise is of the same order of magnitude as the scintillation pulses. If not suppressed properly it can lead to creation of an artificial fast component in a decay spectrum or other distortions of a pulse shape.

Fig. 2 shows an example of a "wrong" event: a scintillation pulse appears after the expected trigger point. A noise peak exceeded the trigger threshold and the event was digitized and stored. The scintillation pulse which coincided with the noise pulse caused that the event passed minimum energy requirement. However, the leading edge of the scintillation pulse is not properly located in the time window.

To properly measure a pulse shape it is important to suppress pile-up of scintillation events within the acquisition window. In Fig. 4 the black line shows a raw signal from the digitizer; the red line shows the signal after low pass filtering and downsampling; the blue line shows the output of a digital constant fraction discriminator (DCFD). There are two points in the figure when the DCFD signal is crossing zero, which indicates that we are dealing with two scintillation pulses. If more then one zero crossing $nZC > 1$ was observed within the acquisition window the event was rejected from further processing. If only one zero crossing was observed the event was kept for further processing, and the zero crossing time was used later for aligning events in time.

3. Results

Fig. 6 shows a pulse height spectrum measured with CsI(Tl) excited with 662 keV γ-photons. The barium X-ray peak was successfully suppressed by the lead absorber, and only Compton scattered events are present besides the 662 keV photopeak. The shown energy range was divided into 10 energy bins and an average pulse shape for each range has been calculated separately.

Fig. 7 shows pulse shapes of CsI(Tl) scintillation measured in multiple energy subranges. The only curve that deviates significantly is for 25–97 keV energies. Another measurement was performed with the requirement that the energy deposit is lower than 184 keV to investigate better the low energy range. Fig. 8 shows the decay curves at low energy deposition. The largest difference was observed for 25–41 keV events, a very small deviation was observed in the 41–89 keV range, and small but still significant pulse change was observed from 89 keV to 184 keV.

To quantify the pulse shape change shown in Fig. 8, the decay curves were fitted with a double exponential function $f(t) = A_1 \exp(-\frac{t}{\tau_1}) + A_2 \exp(-\frac{t}{\tau_2})$, where A_1 and A_2 are the amplitudes of the fast and the slow component, and τ_1 and τ_2 are decay times. The results of these fits are shown in Fig. 9 for the decay times vs energy and Fig. 10 for the intensities I_1 and I_2, which were calculated as follows: $I_i = \frac{A_i * \tau_i}{A_1 * \tau_1 + A_2 * \tau_2}$. Both decay constants are decreasing with decrease of energy, but there is a 'dip' present near 60 keV. The slow component decreases from around 5.8 μs to 4.7 μs in the studied energy range, while the fast component changes from around 900 ns to 850 ns.

The intensity of the slow component I_2 increases with increase of energy, see Fig. 10. The intensity change deviates from being smooth at energies around 50 keV, similarly to the decay components.

Fig. 11 shows a pulse height spectrum measured with a ^{137}Cs source together with X-ray pulses from a pulsed X-ray tube. The tube pulses are observed at equivalent deposited total energy of around 1.3 MeV with FWHM of 37%. Assuming that the average energy of a single X-ray photon from the tungsten anode is around ~10 keV, we may estimate that a single X-ray pulse leads to ~130 detected X-ray photons.

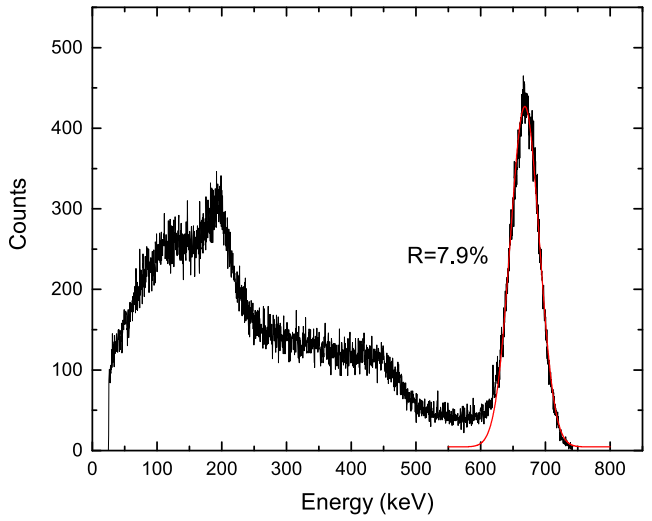

Fig. 6. Pulse height spectrum of ^{137}Cs gamma source measured with CsI:Tl.

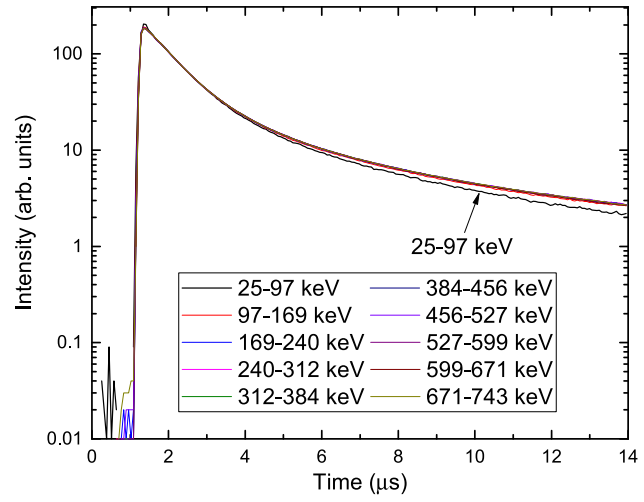

Fig. 7. Energy-sorted pulse shapes of CsI(Tl) under Cs-137 excitation. Only the lowest energy range 25–97 keV displays a significantly different pulse shape. (Color online).

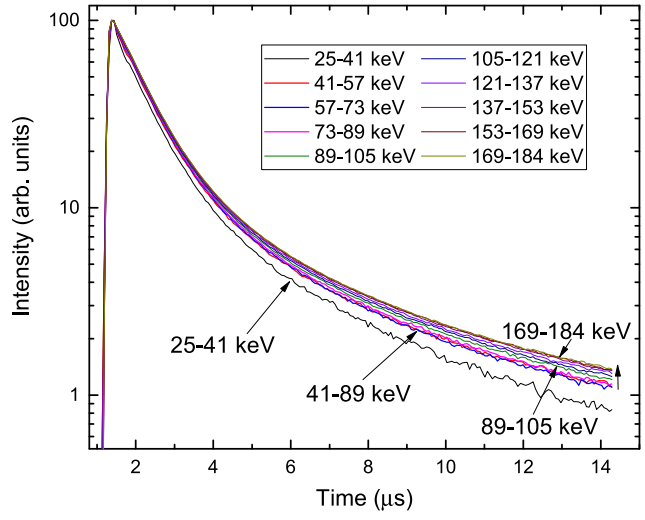

Fig. 8. Energy-sorted pulse shapes of CsI(Tl) under Cs-137 excitation, events with energies lower then 228 keV. (Color online).

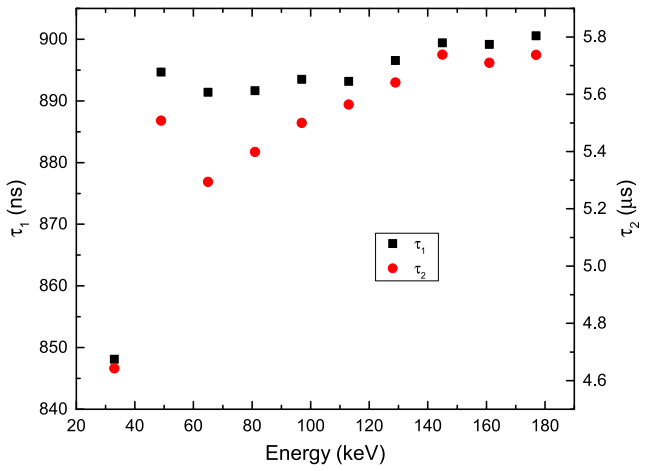

Fig. 9. Decay constants of fast τ_1 and τ_2 slow luminescence decay components.

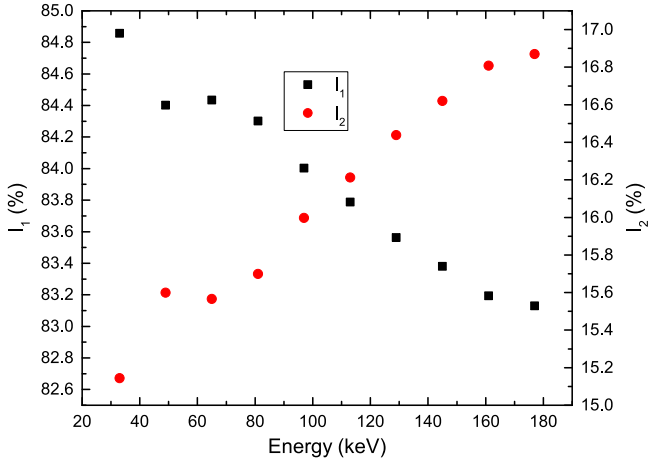

Fig. 10. Intensities of fast I_1 and slow I_2 luminescence decay components.

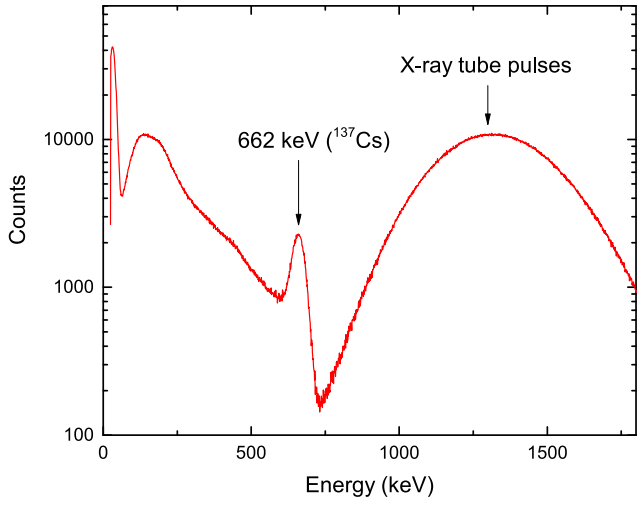

Fig. 11. Pulse height spectrum measured with CsI(Tl) excited with a Cs-137 gamma source and pulsed X-ray tube.

Fig. 12 compares a scintillation pulse shape of CsI(Tl) excited with high energy gamma photons (575–758 keV), low energy Compton electrons (25–96 keV), and pulsed X-rays (10 keV). Events excited by

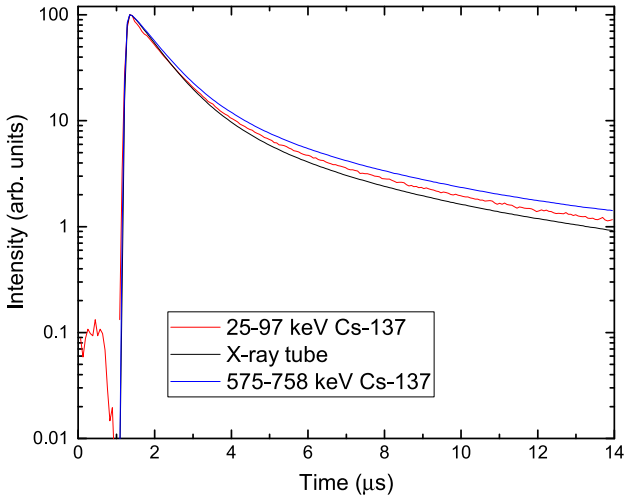

Fig. 12. Comparison of CsI(Tl) scintillation pulse shape excited with Cs-137 gamma source and a pulsed X-ray tube. (Color online).

Table 1
Decay constants and their intensities of CsI(Tl) luminescence excited with a pulsed X-ray tube, low, and high energy excitation.

Excitation	τ_1 (ns)	τ_2 (μs)	I_1 (%)	I_2 (%)
X-rays	800	4.7	87.1	12.9
25–97 keV	845	5.1	83.9	16.1
575–758 keV	850	5.3	82.8	17.2

the pulsed X-ray tube exhibit the lowest intensity of the long decay component, while high energy γ photons have the highest intensity of the slow component. The pulses from Fig. 12 were fitted with a double exponential function and the results are shown in Table 1. The fast component under X-ray excitation is 6% faster compared to the 662 keV energy range. The slow decay constant decreases 11% in the same energy range. The intensity of the slow component increases 4.3% when the source of excitation is changed from 662 keV to X-rays. The pulse change measured with low energy deposition (25–97 keV) compared to the 575–758 keV range is significantly smaller and it is less than 1% change of the fast decay component and less then 4% of the slow component. The change of intensity is around 1%.

The pulse shape factor was defined as a ratio of two integrals: the leading edge, and the tail part of the pulse. Length of both integrals was optimized to get the pulse shape factor value close to one. The integral limits for both edges were 1.92 μs for the early part, and 10.88 μs for the tail part of the pulse. Fig. 13 shows pulse shape factor versus energy of pulses. X-ray pulses (1000–2200 channels) have higher pulse shape factor then γ rays from Cs-137 source (662 keV at 800 channel).

4. Discussion

Lu et al. [6] provided a detailed theoretical analysis of the pulse shape dependence on gamma energy in CsI(Tl). Three possible reactions leading to luminescence were considered. Reaction 1 is the direct Tl^+ excitation by sequential capture of free holes and electrons: $Tl^+ + e^- + h^+ \rightarrow (Tl^+)^* \rightarrow Tl^+ + h\nu$. Reaction 2 is the recombination of self-trapped holes with electrons trapped on Tl^0: $Tl^0 + STH \rightarrow (Tl^+)^*$. Reaction 3 is the thermally activated release of electrons trapped as Tl^0 that subsequently recombine with holes trapped as Tl^{2+}: $Tl^0 + Tl^{2+} \rightarrow (Tl^+)^*$. According to Lu et al., the fast ~ 700 ns decay component can be mostly attributed to the 576 ns radiative decay of $(Tl^+)^*$ created in Reaction 2 and secondarily to a fast component of Reaction 3 found at high excitation densities. The 3- and 17-μs components are the rate- and transport-limited phases, respectively, of Reaction 3 that become more prominent at lower excitation densities. The energy dependence

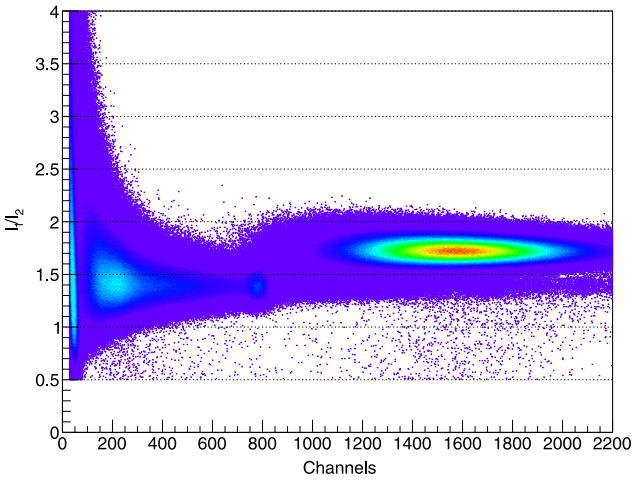

Fig. 13. Pulse shape factor vs pulse integral. Scintillation pulses excited with X-ray tube exhibit a distinctively different shape.

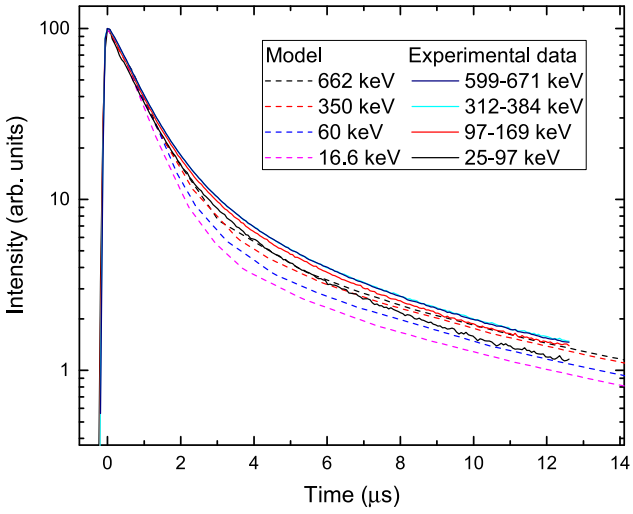

Fig. 14. Comparison of the Lu model predictions [6] with the measured data. (Color online).

of the pulse shape can be explained by the change of efficiency of the Reaction 3 with excitation density, which is dependent on the electric field created between space-separated Tl^0 and Tl^{2+} reservoirs.

Fig. 14 shows a comparison of the theoretical modeling results by Lu [6] and experimental data presented in this work. The model provides a good qualitative description of the data; the same trend and magnitude of the experimental pulse shape change is reproduced by the calculations. However, there are some discrepancies. The model does not predict correctly a change of the slow component (~ 5 μs) decay constant, and the change of the fast component (~ 800 ns) is predicted to be bigger then observed in experiment. Some difficulty for a fair comparison is caused by the fact that the experimental data are measured with limited energy resolution ranges, while theoretical predictions are provided for monoenergetic gamma photons.

5. Conclusions

In this article we have presented a new method of charactering scintillators. We found a weak pulse shape dependence on gamma energy for CsI(Tl), and different scintillation decay time for gamma rays and X-ray pulsed excitations. The experimental results are in good agreement with theoretical predictions by Lu et al. [6], but minor differences are observed and require more research.

Acknowledgments

This work was supported by the Dutch Technology Foundation STW, which is part of the Netherlands Organization for Scientific Research (NWO), which is partly funded by the Ministry of Economic Affairs. This work was partly funded by Saint Gobain Crystals, France.

References

[1] P. Dorenbos, J. de Haas, C. van Eijk, Non-proportionality in the scintillation response and the energy resolution obtainable with scintillation crystals, IEEE Trans. Nucl. Sci. 42 (1995) 2190–2202.

[2] R. Williams, J.Q. Grim, Q. Li, K. Ucer, G. Bizarri, S. Kerisit, F. Gao, P. Bhattacharya, E. Tupitsyn, E. Rowe, et al., Experimental and computational results on exciton/free-carrier ratio,hot/thermalized carrier diffusion, and linear/nonlinear rate constants affecting scintillator proportionality, in: Hard X-ray, Gamma-ray, and Neutron Detector Physics XV, vol. 8852, International Society for Optics and Photonics, 2013, p. 88520J.

[3] J.Q. Grim, K.B. Ucer, A. Burger, P. Bhattacharya, E. Tupitsyn, E. Rowe, V.M. Buliga, L. Trefilova, A. Gektin, G.A. Bizarri, W.W. Moses, R.T. Williams, Nonlinear quenching of densely excited states in wide-gap solids, Phys. Rev. B 87 (2013) 125117.

[4] G. Bizarri, N.J. Cherepy, W.S. Choong, G. Hull, W.W. Moses, S.A. Payne, J. Singh, J.D. Valentine, A.N. Vasilev, R.T. Williams, Progress in studying scintillator proportionality: Phenomenological model, IEEE Trans. Nucl. Sci. 56 (2009) 2313–2320.

[5] X. Lu, Q. Li, G.A. Bizarri, K. Yang, M.R. Mayhugh, P.R. Menge, R.T. Williams, Coupled rate and transport equations modeling proportionality of light yield in high-energy electron tracks: CsI at 295 K and 100 K CsI:Tl at 295 K, Phys. Rev. B 92 (2015) 115207.

[6] X. Lu, S. Gridin, R.T. Williams, M.R. Mayhugh, A. Gektin, A. Syntfeld-Kazuch, L. Swiderski, M. Moszynski, Energy-dependent scintillation pulse shape and proportionality of decay components for csi:tl: Modeling with transport and rate equations, Phys. Rev. Applied 7 (2017) 014007.

[7] L. Dinca, P. Dorenbos, J. de Haas, V. Bom, C.V. Eijk, Alpha–gamma pulse shape discrimination in CsI:Tl, CsI:Na and BaF_2 scintillators, Nucl. Instr. Meth. Phys. Res. A 486 (1–2) (2002) 141–145. Proceedings of the 6th International Conference on Inorganic Scin tillators and their Use in Scientific and Industrial Applications.

[8] M. Kobayashi, Y. Tamagawa, S. Tomita, A. Yamamoto, I. Ogawa, Y. Usuki, Significantly different pulse shapes for γ- and α-rays in $Gd_3Al_2Ga_3O_{12}:Ce^{3+}$ scintillating crystals, Nucl. Instr. Meth. Phys. Res. A 694 (2012) 91–94.

[9] L. Bardelli, M. Bini, P. Bizzeti, F. Danevich, T. Fazzini, N. Krutyak, V. Kobychev, P. Maurenzig, V. Mokina, S. Nagorny, M. Pashkovskii, D. Poda, V. Tretyak, S. Yurchenko, Pulse-shape discrimination with $PbWO_4$ crystal scintillators, Nucl. Instr. Meth. Phys. Res. A 584 (1) (2008) 129–134.

[10] K. Yang, P.R. Menge, V. Ouspenski, Enhanced α - γ discrimination in co-doped $LaBr_3$:Ce, IEEE Trans. Nucl. Sci. 63 (2016) 416–421.

[11] S. Rawat, M. Tyagi, P. Netrakanti, V. Kashyap, A. Singh, D. Desai, A. Mitra, G.A. Kumar, S. Gadkari, Pulse shape discrimination properties of $Gd_3Ga_3Al_2O_{12}$:Ce,B single crystal in comparison with CsI:Tl, Nucl. Instr. Meth. Phys. Res. A (2016) pp. –.

[12] K. Mesick, D. Coupland, L. Stonehill, Pulse-shape discrimination and energy quenching of alpha particles in $Cs_2LiLaBr_6:Ce^{3+}$, Nucl. Instr. Meth. Phys. Res. A 841 (2017) 139–143.

[13] N. Zaitseva, B.L. Rupert, I. Paweczak, A. Glenn, H.P. Martinez, L. Carman, M. Faust, N. Cherepy, S. Payne, Plastic scintillators with efficient neutron/gamma pulse shape discrimination, Nucl. Instr. Meth. Phys. Res. A 668 (Supplement C) (2012) 88–93.

[14] P. Belli, R. Bernabei, R. Cerulli, C. Dai, F. Danevich, A. Incicchitti, V. Kobychev, O. Ponkratenko, D. Prosperi, V. Tretyak, Y. Zdesenko, Performances of a CeF_3 crystal scintillator and its application to the search for rare processes, Nucl. Instr. Meth. Phys. Res. A 498 (1–3) (2003) 352–361.

[15] R. Ogawara, M. Ishikawa, Feasibility study on signal separation for spontaneous alpha decay in $LaBr_3$:Ce scintillator by signal peak-to-charge discrimination, Rev. Sci. Instrum. 86 (8) (2015).

[16] C.M. Whitney, L. Soundara-Pandian, E.B. Johnson, S. Vogel, B. Vinci, M. Squillante, J. Glodo, J.F. Christian, Gamma–neutron imaging system utilizing pulse shape discrimination with clyc, Nucl. Instr. Meth. Phys. Res. A 784 (Supplement C) (2015) 346–351. Symposium on Radiation Measurements and Applications 2014 (SORMA XV).

[17] R. Cerulli, P. Belli, R. Bernabei, F. Cappella, F. Nozzoli, F. Montecchia, A. d'Angelo, A. Incicchitti, D. Prosperi, C. Dai, Performances of a baf2 detector and its application to the search for decay modes in 130ba, Nucl. Instr. Meth. Phys. Res. A 525 (3) (2004) 535–543.

[18] A. Syntfeld-Każuch, M. Moszyński, L. Świderski, W. Klamra, A. Nassalski, Light pulse shape dependence on γ-ray energy in CsI(Tl), IEEE Trans. Nucl. Sci. 55 (2008) 1246–1250.

[19] W.-S. Choong, G. Bizarri, N. Cherepy, G. Hull, W. Moses, S. Payne, Measuring the dependence of the decay curve on the electron energy deposit in NaI(Tl), Nucl. Instr. Meth. Phys. Res. A 646 (1) (2011) 95–99.

[20] X. Wen, A. Enqvist, Measuring the scintillation decay time for different energy deposited by γ -rays and neutrons in a $Cs_2LiYCl_6:Ce^{3+}$ detector, Nucl. Instr. Meth. Phys. Res. A 853 (Supplement C) (2017) 9–15.

[21] L. Świderski, n. Marek Moszy, A. Syntfeld-Każuch, M. Szawlowski, T. Szcześniak, Measuring the scintillation decay time for different energy depositions in NaI:Tl, LSO:Ce and $CeBr_3$ scintillators, Nucl. Instr. Meth. Phys. Res. A 749 (Supplement C) (2014) 68–73.

[22] S.W. Smith, The Scientist and Engineer's Guide To Digital Signal Processing, California Technical Publishing, San Diego, CA, USA, 1997.